

Investigations of structural, optical, and photovoltaic properties of Fe-alloyed ZnS quantum dots

Sabit Horoz¹ · Omer Sahin²

Received: 23 December 2016 / Accepted: 3 March 2017 / Published online: 15 March 2017
© Springer Science+Business Media New York 2017

Abstract Pure ZnS and Fe-alloyed ZnS quantum dots (QDs) prepared by wet-chemical method at room temperature using mercaptoethanol as a capping agent. The nominal concentrations of Fe were 5, 10, and 15% weight of Fe. The QDs were characterized by X-ray diffraction (XRD), scanning electron microscope (SEM), energy dispersive analysis of X-rays (EDAX), optical absorption and photoluminescence (PL) measurements. The cubic phase of pure and Fe-alloyed ZnS QDs was indicated using the XRD measurements. It was determined that the sizes of doped samples decrease as the Fe concentrations are increased. The band gaps of QDs were investigated using optical measurements. It was observed that the band gaps and the absorption windows of Fe-alloyed ZnS QDs increase with the increase in the concentrations of Fe. It was seen that as the concentration of Fe increases, both the absorption and the emission peaks of the alloyed ZnS QDs shift to shorter wavelength. The photovoltaic properties of Fe alloyed ZnS QDs have been investigated in this study for the first time. The pure ZnS and Fe-alloyed ZnS QDs were used to make quantum dots-sensitized solar cells. The performances of the solar cells, with the short circuit current density (J_{SC}) and open circuit voltage (V_{OC}) and incident photon to electron conversion efficiency (IPCE) of Fe-alloyed ZnS QDs increased with increasing Fe doping. Thus, Fe-alloyed ZnS QDs can be used as promising materials in solar cell technology due to fact that they have wider optical absorption spectrums.

1 Introduction

II–VI semiconductor quantum dots (QDs) demonstrate interesting size dependent electrical and optical properties. Owing to their unique properties, they have received great attention during past decades and have been used in many applications in modern technologies such as photovoltaics (PVs), light emitting diodes (LEDs), and nano-lasers [1–5]. Among these II–VI semiconductors, Zinc Sulfide (ZnS) is an extensive semiconductor that has a relatively large direct band gap of 3.54 eV [6–9] which has been widely studied as an important phosphor for promising applications in optoelectronics, photonics, and PVs [10, 11]. In comparison to bulk ZnS, ZnS QDs especially show size dependent optical properties due to quantum confinement effect when the radius of the particles is closer to or smaller than the exciton Bohr radius. It means that the bandgap of ZnS QDs can be directly tuned by particle size [9].

Another method to control the electrical and optical properties is doping which introduces traps and discrete energy levels in the band gap for excited electrons [12–16]. Transition metals such as Mn [17], Cu [18], Fe [19], Co [20], and Ni [21] have been extensively used as dopants by researchers. Bharvaga et al. [17] reported Mn²⁺ doped ZnS QDs show a high quantum efficiency of Mn²⁺ which was one of the early investigations on doped semiconductor QDs. They concluded that Mn²⁺ has an emission at 585 nm (2.12 eV) arising from the ⁴T₁–⁶A₁ d–d spin forbidden electronic transition of Mn²⁺. In such studies on the Mn-doped ZnS, Fe-doped ZnS synthesized by various techniques has been widely investigated. For instance, Kashyout et al. [19] made ZnFeS thin films by electrochemical deposition on tin oxide substrates, and then they reported that the bandgaps of thin films increase with Fe content in ZnFeS thin film. This main result also has been proved by

✉ Sabit Horoz
sabithoroz@siirt.edu.tr

¹ Department of Physics, Siirt University, 56100 Siirt, Turkey

² Department of Chemical Engineering, Siirt University, 56100 Siirt, Turkey

different researchers who synthesized Fe-doped ZnS with different methods [22, 23]. Moreover, two different structures (cubic and hexagonal) of Fe-doped ZnS were reported by different researchers; Akhtar et al. [24] and Li et al. [25] reported that Fe doped ZnS shows cubic structure while Kumar et al. [19] and Abdullah et al. [26] informed that Fe doped ZnS indicates hexagonal structure.

From the application view, there are limited studies on the photovoltaic applications of doped ZnS QDs while un-doped and doped II–VI semiconductor QDs have been widely used as sensitizers in quantum dot sensitized solar cells (QDSSCs) applications [12, 27, 28]. In our previous studies [29, 30], we reported alternative QDs prepared using co-precipitation method (Mn doped ZnS and Eu doped ZnS) to improve IPCE values of quantum dots sensitized solar cells because the absorption windows of ZnS QDs were enhanced by Mn and Eu doping. To the best of our knowledge, there is no report on the photovoltaic properties of Fe-doped ZnS QDs. Therefore, this study is thought to be original.

QDs can be synthesized by several well-known techniques. Spin coating [31], hydrothermal [32], physical/thermal evaporation [33, 34], pulsed laser ablation/ deposition [27, 28], wet-chemical [35], chemical bath deposition [36] and SILAR [12] are some them. The wet-chemical is one these methods, is one of the most appropriate methods due to its simplicity and ease. The wet-chemical technique is a low-cost method and requires ambient environmental conditions and simple lab equipment. Many samples can be prepared by the wet-chemical method within a few hours.

In our present study, the effects of Fe content on the photovoltaic properties of ZnS QDs are discussed for the first time. The synthesis and characterizations of pure ZnS and Fe-alloyed ZnS QDs have been reported, prepared by the wet-chemical method at room temperature using the mercaptoethanol as a capping agent. Their structural, optical, and photovoltaic properties have been studied.

2 Experimental details

Pure ZnS and Fe-alloyed ZnS QDs have been synthesized at room temperature by the wet-chemical method using mercaptoethanol as a capping agent which has been used to prevent any agglomeration during the preparation. Zn acetate di-hydrate as Zn sources, Fe chloride as Fe source, sodium sulfide as S source have been used without any further purification to prepare pure ZnS and Fe-alloyed ZnS QDs. In typical wet-chemical method, two clean beakers were used to prepare appropriate amount of aqueous solutions of cation source which is the Zn (CH_3COO). $2\text{H}_2\text{O}$ and anion source were Na_2S . Then, these two solutions were transferred into a third clean beaker, then stirred for

a certain time to get a homogeneous mixture at room temperature. The mercaptoethanol (2 ml) was added onto the mixture as the stirring process continued. A filter paper was used to separate the precipitated sample from the solution. The resulting particles were washed in water and ethanol a few times to get rid of unwanted compounds inside the particles. The final solution was heated in an oven a certain temperature. Then, a mortar was used to grind the obtained powders to get ZnS QDs.

For preparing Fe-alloyed ZnS QDs, the appropriate amounts of FeCl_2 was added to the solution of Zn (CH_3COO). $2\text{H}_2\text{O}$, the same procedure was followed.

X-ray diffraction (XRD) on a Rigaku X-ray diffractometer with Cu K_α ($\lambda = 154,059$ pm) radiation and scanning electron microscope (SEM) (JEOL JSM 5800) were used to analyze structural and morphological properties of pure ZnS and Fe-alloyed ZnS QDs, respectively. UV–Vis and photoluminescence (PL) spectra of pure ZnS and Fe-alloyed ZnS QDs were obtained with a Perkin-Elmer Lambda 2 and a Perkin-Elmer LS 50B, respectively. Incident photon to electron conversion efficiency (IPCE) and current density (J) versus voltage (V) measurements were performed by using PCE-S20 with a monochromatic light source consisting of a 150-W Xe lamp and a monochromator. For IPCE and J–V measurements, fluorine doped tin oxide (FTO, $13\Omega \text{ sq}^{-2}$) conductive glass substrates were used as the photo electrodes. The TiO_2 nanowires (NWs) were coated on the FTO substrates using the doctor blade method, then sintered at 450°C for 45 min. A suspension of pure ZnS and Fe-alloyed ZnS QDs were dropped on the FTO substrates with the TiO_2 NWs. The substrates were dried with N_2 gas and secured against Cu_2S counter electrodes containing polysulfide electrolytes.

3 Discussion and results

XRD measurements have been used to analyze the structural properties of pure ZnS and Fe-alloyed ZnS QDs. Figure 1a, b, c indicate the XRD patterns for pure ZnS, Fe (5%): ZnS, Fe (10%): ZnS and Fe (15%): ZnS QDs prepared by wet-chemical method at room temperature, respectively.

All peaks of pure ZnS and Fe-alloyed ZnS QDs can be identified as those of zinc blende crystal structure (JCPD No: 65-9585) of ZnS, which correspond to the (111), (220), and (311) planes. No extra peaks have been observed which confirm that the Fe ions have been substituted in ZnS lattice and the formation of Fe compounds or Fe oxides have been ruled out in Fe-alloyed ZnS QDs. The peak positions of pure and Fe-alloyed ZnS QDs are shown in Table 1.

It can be clearly seen from the Table 1 that the diffraction peaks of QDs slightly shift towards the lower Bragg's

Fig. 1 **a** XRD patterns of pure ZnS and Fe (5%): ZnS QDs synthesized at room temperature, **b** XRD patterns of pure ZnS and Fe (10%): ZnS QDs synthesized at room temperature, **c** XRD patterns of pure ZnS and Fe (15%): ZnS QDs synthesized at room temperature

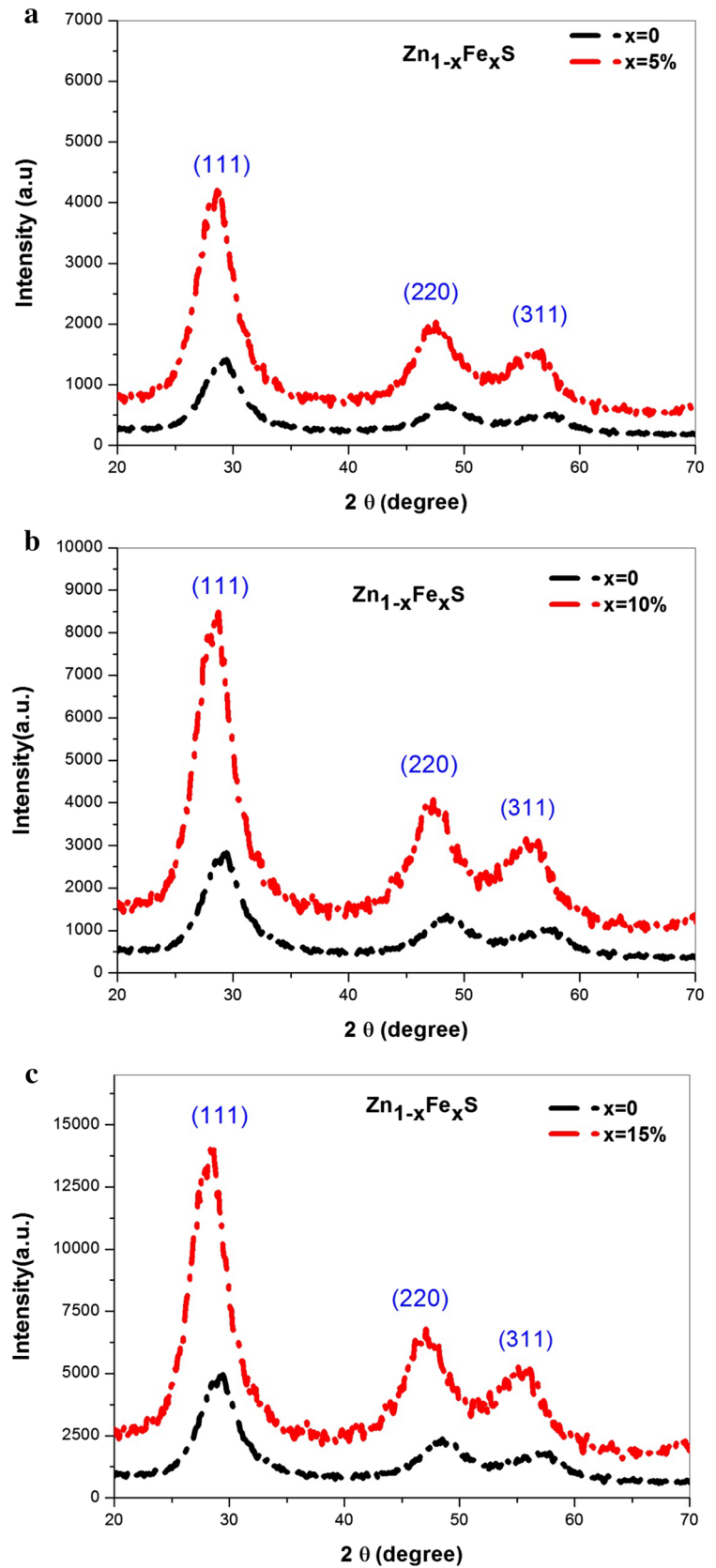


Table 1 The diffraction peaks pure ZnS and Fe (5%, 10%, 15%): ZnS QDs correspond to (111), (220), and (311) planes

Planes	2θ (degree) for ZnS QDs	2θ (degree) for Fe(5%): ZnS QDs	2θ (degree) for Fe(10%): ZnS QDs	2θ (degree) for Fe(15%): ZnS QDs
(111)	29.32	28.80	28.54	28.41
(220)	48.63	47.32	47.19	47.06
(311)	57.10	56.06	55.79	55.41

angle when ZnS QDs are alloyed with different concentration of Fe. It refers that Fe^{2+} ions lower the lattice distance of the ZnS crystal due to the larger radius of Zn^{2+} (0.74 Å) than that of the Fe^{2+} ion when Fe^{2+} is included into the lattice of the ZnS crystal.

All broad peaks of pure ZnS and Fe-alloyed ZnS QDs exhibit that the sizes of the pure ZnS and Fe-alloyed ZnS QDs become smaller. The average particle sizes of the QDs were estimated from the peak widths of the relatively strong (111), (220), and (311) diffractions using Scherrer's formula as given in Eq. 1

$$d = 0.9\lambda / (\beta \cos \theta) \quad (1)$$

where d is the mean size of the QDs, λ is the wavelength of X-ray, β is the broadening measured as the full width at half maximum (FWHM) in radians, and θ is Bragg's diffraction

angle. The sizes of pure ZnS, Fe (5%)—alloyed ZnS, Fe (10%)—alloyed ZnS and Fe (15%)—alloyed ZnS QDs found from the XRD peak width are 2.52, 2.32, 2.25, and 2.08 nm, respectively. This result which is consistent with the investigations of Li et al. [25] shows that the decrease in particle size is clearly from the increase in the β of the XRD peaks of the QDs due to the size effect.

Figure 2a, b, c, d demonstrate the SEM images of pure ZnS and Fe (5%, 10%, 15%)—alloyed ZnS QDs prepared by wet-chemical method at room temperature, respectively. It is confirmed that pure ZnS and Fe (5%, 10%, 15%)—alloyed ZnS QDs have a cubic structure which is consistent with data obtained from XRD measurement but the pure ZnS QDs has more agglomeration than Fe (5%, 10%, 15%)—alloyed ZnS QDs. It can be seen that Fe alloying is clearly observed.

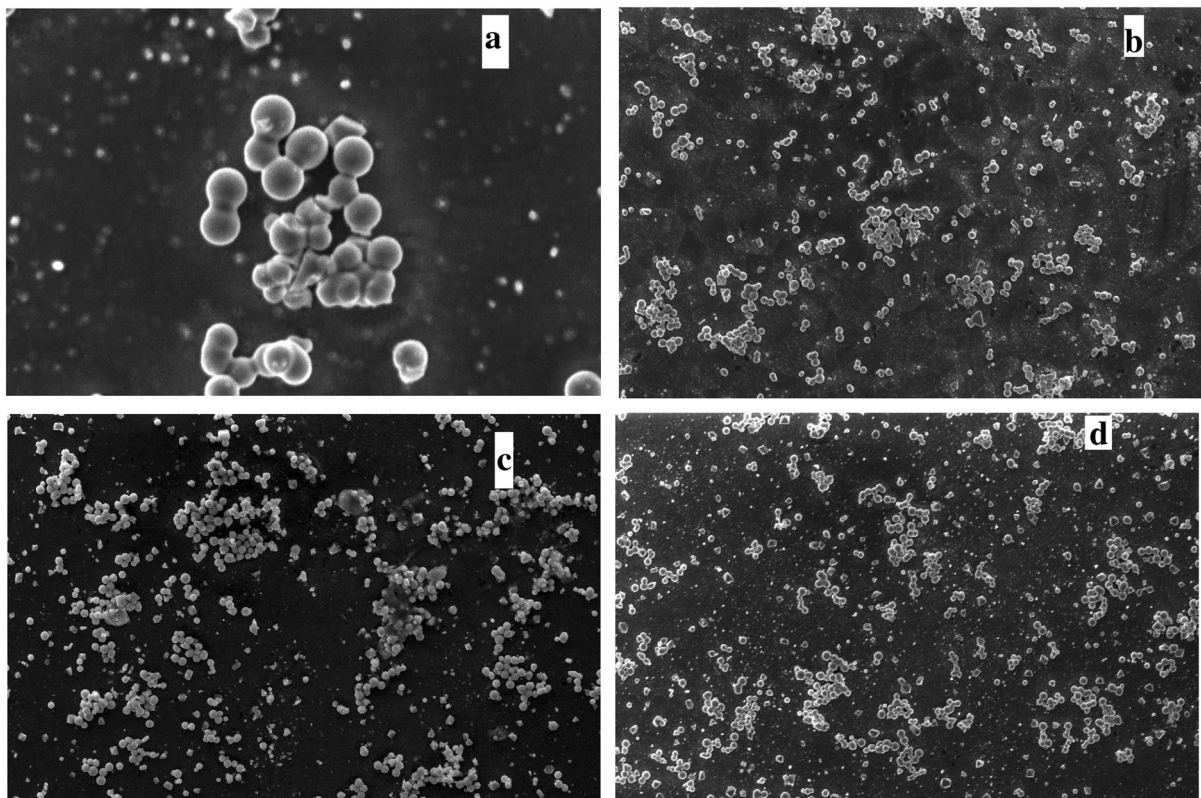
**Fig. 2** SEM images of (a) pure ZnS QDs (b–d) Fe (5%, 10%, 15%)—alloyed ZnS QDs synthesized at room temperature

Table 2 Comparison of nominal and observed Fe concentrations in ZnS

Samples	Nominal Fe %	Observed Fe %
Pure ZnS QDs	0	0
Fe-alloyed ZnS QDs (1)	5	3.65
Fe-alloyed ZnS QDs (2)	10	8.1
Fe-alloyed ZnS QDs (3)	15	11.1

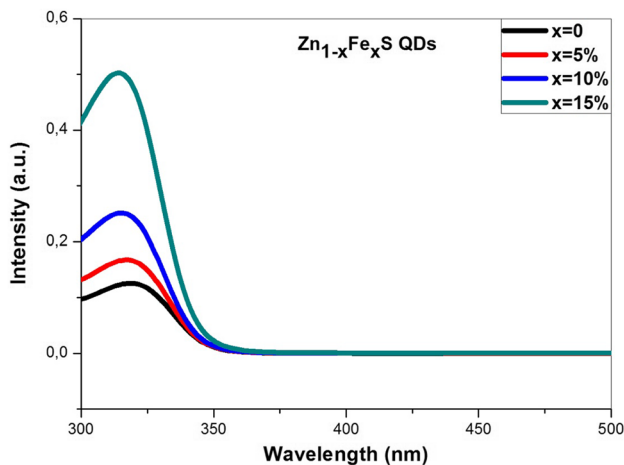


Fig. 3 The UV–Vis absorption spectra of pure ZnS and Fe-alloyed ZnS QDs synthesized at room temperature

Table 3 Comparison E_g values and particle sizes for pure ZnS and Fe-alloyed ZnS QDs using peak positions obtained from the optical spectra

Samples	Peak positions (nm)	E_g (eV)	Particle sizes (nm)
ZnS QDs	320	3.88	2.52
Fe (5%): ZnS QDs	317.2	3.91	2.40
Fe (10%): ZnS QDs	315.3	3.93	2.33
Fe (15%): ZnS QDs	313.5	3.96	2.27

The energy dispersive analysis of X-rays (EDAX) spectrum was used to confirm the real alloying percentage of Fe ions in ZnS. Table 2 shows the observed percentage Fe ions and nominal percentages of Fe ions which have been used in the preparation. The EDAX spectrums indicate the presence of Fe ions in ZnS. The observed percentage of Fe is less than nominal percentages. The reason behind this loss may be attributed to the washing of samples during the preparation.

Figure 3 shows the optical absorption spectra of pure ZnS and Fe-alloyed ZnS QDs prepared by wet-chemical method at room temperature.

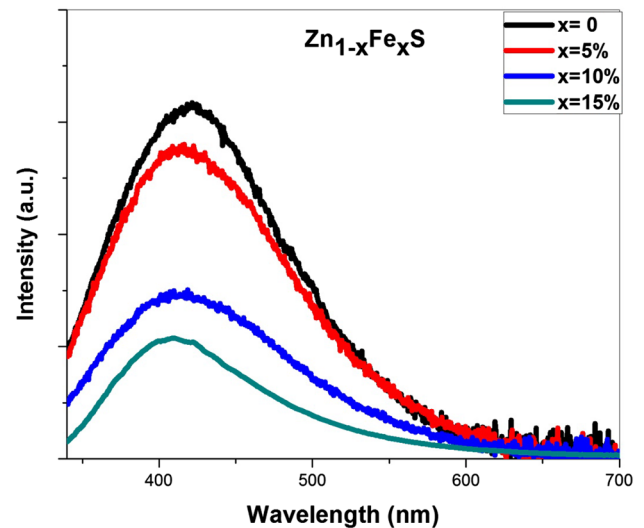


Fig. 4 The Photoluminescence (PL) spectra for pure ZnS and Fe-alloyed ZnS QDs synthesized at room temperature

There are two observations on the optical spectra of samples as indicated in Fig. 3. The first one is that the blue shift in the peak positions, from 320 to 313, 2 nm, was observed as the Fe concentrations were increased from 0 to 15%. From the peak positions, the band gap (E_g) values of the QDs were obtained and using these values, the particle sizes were calculated using the formula given in ref [37]. The Table 3 shows the E_g values and the sizes of pure ZnS and Fe-alloyed ZnS QDs. It is clear that the particle sizes decrease with the increase in the band gap of the QDs due to the quantum confinement effect. The similar observation was obtained by Kumar et al. [23]. The mechanism of size reduction by Fe doping needs to be studied. The sizes obtained from UV–Vis spectra were close to values obtained from XRD data.

The second observation is that the spectral response range of the Fe-alloyed ZnS QDs was wider than pure ZnS QDs. It may be attributed to introduction of Fe impurities which improves the spectral response of the ZnS QDs in the visible range. Due to this property, Fe-alloyed ZnS QDs can be effectively used as sensitizers in solar cells technologies.

Synthesis conditions, shape, size, and energetic position of the surface states affect the photoluminescence (PL) emission of the QDs. Figure 4 shows the room temperature PL spectra, under 310 nm excitation, for pure ZnS and Fe-alloyed ZnS QDs prepared by the wet-chemical method at room temperature. The broad emission peaks which are related to radiative recombination involving defect states (due to absence of Zn^{2+} or S^{2-} ions in ZnS lattice), are located at about 412 nm for pure ZnS QDs, 416, 412, and 408 nm for Fe (5%, 10%, and

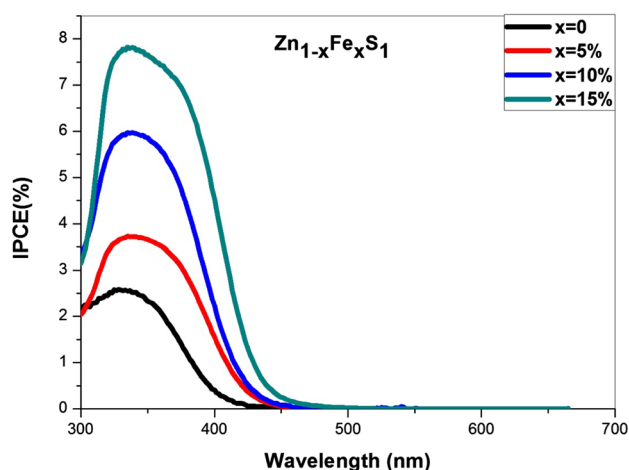


Fig. 5 The IPCE spectra of pure ZnS and Fe-alloyed ZnS with different Fe concentrations attached to TiO₂ NWs

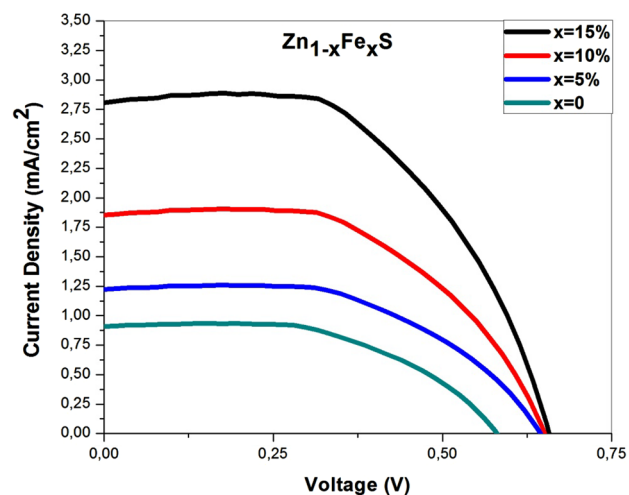


Fig. 6 J–V plots of pure and Fe (5%, 10%, 15%)-alloyed ZnS QDSSCs

15%)—alloyed ZnS QDs, respectively. We should note that the main effect of the Fe doping on the PL spectra of the ZnS QDs is that the PL peaks slightly shift to shorter wavelengths with increasing Fe doping. This result is also consistent with that obtained from the UV–Vis spectra

shown in Fig. 3. In other words, the reduction size of ZnS QDs size caused a blue shifted of the PL spectra of ZnS QDs as consequence of the quantum confinement effect.

Figures 5 and 6 indicate the IPCE spectra and current density (J) versus voltage (V) curves for devices fabricated with pure ZnS and Fe-alloyed ZnS QDs. There are two main points were observed from the Fig. 5, which are in total agreement with the absorption spectra. Firstly, the IPCE value increased with increasing the Fe concentrations. The obtained maximum IPCE value was 4.5% for Fe (15%): ZnS QDs while the value was about 0.5% for pure ZnS QDs. It is no wrong say that this result supports our previous studies [25, 26] on the photovoltaic properties of alloyed ZnS QDs. Secondly, when the Fe concentrations were increased in ZnS QDs, the IPCE peaks of the QDs $\lambda < 350$ nm were blue shifted due to the quantum size effect on the ZnS QDs while the IPCE spectrum edges were red shifted due to the introduction of Fe ions in ZnS QDs which enhance the spectral response of the ZnS QDs [30].

It is an important note that there was a significant improvement in the performance of the ZnS QDs (shown in Fig. 6) when they were alloyed with different concentrations of Fe. The power efficiencies shown in Table 4 were found 2, 1.32, 0.82, and 0.6 for pure ZnS and Fe (5%, 10%, 15%)-alloyed ZnS QDs, respectively.

The effects of Fe doping on the performance of the ZnS QDSSCs could be arrayed; (1) the spectral response of the ZnS QDs enhances as the Fe concentrations are increased (shown in Fig. 3). This enhancement causes a significant improvement on the current density. (2) Fe-doped ZnS QDs has a higher crystal quality than pure ZnS (shown in Fig. 2). The improvement in the crystalline will reduce the recombination of photo-excited carriers and this effect will increase the power conversion efficiency. (3) The contact between working electrode and QD sensitizers plays an important role to enhance the efficiency of QDSSCs. Due to Fe alloying, the contact between ZnS QDs and TiO₂ NW becomes good. Thus, this contact can block the interfacial recombination of the injected transfer from NWs to polysulfide electrolytes. Correspondingly, it improves the performance of the ZnS QDSSCs [38].

Table 4 Comparison of V_{OC} , J_{SC} , and η of un-doped and Fe (5%, 10%, 15%)—alloyed ZnS QDSSCs prepared at room temperature

Samples	Open circuit voltage (V_{OC}) (V)	Short circuit current density (J_{SC}) (mA/cm ²)	Power conversion efficiency (η) (%)
Pure ZnS QDs	0.58	0.91	0.6
Fe (5%)—alloyed ZnS QDs	0.64	1.25	0.82
Fe (10%)—alloyed ZnS QDs	0.65	1.88	1.32
Fe (15%)—alloyed ZnS QDs	0.66	2.81	1.6

4 Conclusions

In this study, pure ZnS and Fe-alloyed ZnS QDs were successfully synthesized by wet-chemical method at room temperature using the mercaptoethnaol as a capping agent. The structural morphological and optical properties of pure ZnS and Fe-alloyed ZnS QDs have been evaluated by the XRD, SEM, UV–Vis, and PL spectra. The particle sizes of cubic phase of pure ZnS and Fe-alloyed ZnS QDs have been calculated using the values obtained from the XRD and the optical spectra. The sizes obtained from two different measurements are in good agreement with each other. Based on the UV–Vis and PL measurements, it was observed that first; the E_g values of the ZnS QDs increase as the Fe concentrations are increased and second; the spectral response of Fe-alloyed ZnS QDs is wider than pure ZnS QDs. The photovoltaic applications of Fe-alloyed ZnS QDs have been investigated in this study for the first time. It was clearly observed that the Fe-alloyed ZnS QDs exhibit increment in the IPCE and the power conversion efficiency compare pure one. Thus, Fe-alloyed ZnS QDs has enabled us to achieve a significant improvement in QDSSCs. They can be also used promising materials in solar cell technology due to the fact that they have wider optical absorption spectra.

References

1. R. Vogel, K. Pohl, H. Weller, Chem. Phys. Lett. **174**, 241 (1990)
2. L. Li, X. Yang, J. Gao, H. Tian, J. Zhao, A. Hagfeldt, L. Sun, J. Am. Chem. Soc. **133**, 8458 (2011)
3. K.S. Leschkes, R. Divakar, J. Basu, E. Enache-Pommer, J.E. Boercker, C.B. Carter, U.R. Kortshagen, D.J. Norris, E.S. Aydil, Nano Lett. **7**, 1793 (2007)
4. I.J. Kramer, E.H. Sargent, ACS Nano **5**, 8506 (2011)
5. B.R. Sankapal, S.D. Sartale, C.D. Lokhande, A. Ennaoui, Sol. Energy. Mater. Sol. Cells **83**, 447 (2004)
6. P. Yang, M. Lu, D. Xu, D. Yuan, C. Song, G. Zhou, Chem. Phys. Lett. **336**, 78 (2001)
7. H. Hu, W. Zhang, Opt. Mater. **28**, 550 (2006)
8. Y.Q. Li, J.A. Zapien, Y.Y. Shan, Y.K. Liu, S.T. Lee, Appl. Phys. Lett. **88**, 013115 (2006)
9. H.Y. Xu, Y.C. Liu, C.S. Xu, Y.X. Liu, C.L. Shao et al., J. Chem. Phys. **124**, 074707 (2006)
10. N. Karar, F. Singh, B.R. Mehta, J Appl. Phys. **95**, 656 (2004)
11. L. Wang, X. Xu, X. Yuan, J. Lumin. **130**, 137 (2010)
12. P.K. Santra, P.V. Kamat, J. Am. Chem. Soc. **134**, 2508 (2012)
13. A. Sobhani-Nasab, M. Behpour, J. Mater. Sci: Mater. Electron **27**, 11951 (2016)
14. S.M. Hosseinpour-Mashkani, A. Sobhani-Nasab, J. Mater. Sci. **27**, 7553 (2016)
15. S.M. Hosseinpour-Mashkani, M. Maddahfar, A. Sobhani-Nasab, J. Mater. Sci. **27**, 480 (2016)
16. M. Rahimi-Nasrabadi, M. Behpour, A. Sobhani-Nasab, S.M. Hosseinpour-Mashkani, J. Mater. Sci. **26**, 9781 (2015)
17. R.N. Bhargava, D. Gallagher, X. Hong, A. Nurmikko, Phys. Rev. Lett. **72**, 416 (1994)
18. G.S. Harrish, P.S. Reddy, Phys. B: Condens. Mater. **473**, 53 (2015)
19. A.B. Kashyout, A.S. Arich, N. Giordano, V. Antonucci, Mater. Chem. Phys. **41**, 60 (1995)
20. J.K. Salem, T.M. Hammad, M.A. Draaz, S. Kuhn, and R. Hempelmann, J. Mater. Sci. Mater. Electron **25**, 2177 (2014)
21. H. Soni, M. Chawda, D. Bodas, Mater. Lett. **63**, 769 (2009)
22. F. Zhu, S. Dong, and G. Yang, Optoelectron. Adv. Mater—Rapid. Commun. **4**, 2075 (2010)
23. S. Kumar, N.K. Verma, J. Mater. Sci: Mater. Electron. **26**, 2759 (2015)
24. M. S. Akhtar, M. A. Malik, Y. G. Alghamdi, K. S. Ahmad, S. Riaz, and S. Naseem, Mater. Sci. Semicond. Process **39**, 291 (2015)
25. Y. Li, C. Cao, Z. Chen, Chem. Phys. Lett. **517**, 58 (2011)
26. H. Abdullah, S. Selman, A. Roslan, S. Shaari, M.M. Salleh, J.S. Mandeep, in *NANOTECHNOLOGY'10 Proceedings of the 2nd WSEAS international conference on Nanotechnology*, 191–194
27. Q. Dai, J. Chen, L. Lu, J. Tang, W. Wang, Nano Lett. **12**, 4187 (2012)
28. S. Horoz, L. Liu, Q. Dai, B. Yakami, J.M. Pikal, W. Wang, J. Tang, Appl. Phys. Lett. **101**, 223902 (2012)
29. S. Horoz, Q. Dai, F. S. Maloney, B. Yakami, J.M. Pikal, X. Zhang, J. Wang, W. Wang, and J. Tang, Phys. Rev. Appl. **3**, 024011 (2015)
30. S. Horoz, B. Yakami, U. Poudyal, J. M. Pikal, W. Wang, and J. Tang, AIP Adv. **6**, 045119 (2016)
31. C.-F. Lin, E.-Z. Liang, S.-M. Shih and W.-F. Su, In Symposium on Integrated Optoelectronic Devices; International Society for Optics and Photonics, **102** (2002)
32. W.-W. So, J.-S. Jang, Y.-W. Rhee, K.-J. Kim, S.-J. Moon, J. Colloid Interface Sci. **237**, 136 (2001)
33. A. Pan, H. Yang, R. Liu, R. Yu, B. Zou, Z. Wang, J. Am. Chem. Soc. **127**, 15692 (2005)
34. L.M. Yu, C.C. Zhu, X.H. Fan, L.J. Qi, W. Yan, J. Zhejiang Univ. Sci. A **7**, 1956 (2006)
35. R. Kripal, A.K. Gupta, S.K. Mishta, K. Srivastava, A.C. Pandey, S.G. Prakash, Spectrochim. Acta. Part. A **76**, 523 (2010)
36. C.G. Lazos, E. Rosendo, H. Juarez, G.G. Salgado, T. Diaz, M.R. Falfan, A.I. Olivia, P. Quintana, D.H. Aguilar, W. Cauich, J. Electrochem. Soc. **155**, 158 (2008)
37. L. Brus, J. Phys. Chem **90**, 2555 (1986)
38. Y. Li, L. Wei, R. Zhang, Y. Chen, L. Mei, J. Jiao, Nanoscale. Res. Lett. **8**, 89 (2013)